

1 **Chemical imaging of heterogeneous muscle foods by NIR hyperspectral imaging in**  
2 **transmission mode**

3

4 Jens Petter Wold<sup>a,\*</sup>, Martin Kermit<sup>b</sup>, Vegard Herman Segtnan<sup>c</sup>

5

6

7 a – Nofima, Norwegian Institute for Food and Fisheries Research, Muninbakken 9-13,  
8 Breivika, NO-9291 Tromsø, Norway

9

10 b – Norwegian Computing Center, Gaustadalléen 23A, 0373 Oslo, Norway

11

12 c – Orkla Foods, Lienga 6, 1414 Trollåsen, Norway

13

14

15 \*Corresponding author:

16 Jens Petter Wold

17 Nofima AS

18 Osloveien 1

19 1430 Ås

20 Tel: +47 95979749

21 Fax: +47 64970333

22 jens.petter.wold@nofima.no

23

24 **Abstract**

25 Foods and biomaterials are in general heterogeneous and it is often a challenge to obtain  
26 spectral data which is representative for the chemical composition and distribution. This paper  
27 presents a setup for NIR transmission imaging where the samples are completely  
28 transilluminated, probing the entire sample. The system measures falling samples at high  
29 speed and consists of an NIR imaging scanner covering the spectral range 760 – 1040 nm and  
30 a powerful line light source. The investigated samples were rather big; whole pork bellies of  
31 thickness up to 5 cm, salmon fillets with skin and 3 cm thick model samples of ground pork  
32 meat. Partial least square regression models for fat were developed for ground pork and  
33 salmon fillet with high correlations ( $R=0.98$  and  $R=0.95$ , respectively). The regression models  
34 were applied at pixel level in the hyperspectral transmission images and resulted in images of  
35 fat distribution where also deeply embedded fat clearly contributed to the result. The results  
36 suggest that it is possible to use transmission imaging for rapid, non-destructive and  
37 representative sampling of very heterogeneous foods. The proposed system is suitable for  
38 industrial use.

39

40 **Key words:** NIR spectroscopy; Near-infrared spectroscopy; hyperspectral imaging;  
41 transmission measurements; multivariate regression; chemical imaging; pork bellies; salmon  
42 fillets; heterogeneous samples; fat distribution

43

44

## 45 **Introduction**

46 Near infrared (NIR) hyperspectral imaging is becoming increasingly established as a feasible  
47 method for detailed non-destructive chemical studies of materials. One of the areas where this  
48 technology has proven to be useful is within analysis of biochemical distribution at either  
49 micro or macro level. Hyperspectral imaging is also used industrially for on-line quality  
50 control of foods and offers several advantages over conventional spectroscopy. Imaging  
51 provides spatial information and enables detection of local features of interest, such as for  
52 instance blood spots<sup>1</sup>, parasites<sup>2</sup> or oxidation.<sup>3</sup> In the food industry it is often required to  
53 quantify the chemical composition and distribution in every product on the line. The ability to  
54 quantify and map fat in fish fillets is for instance useful for subsequent classification and  
55 sorting.<sup>4</sup> The same can be the case for quality grading of meat trimmings according to  
56 distribution of fat, lean muscle and connective tissue.<sup>5,6</sup>

57 Foods are heterogeneous, and measurement or imaging of the surface of the product is not  
58 always representative of the entire product. NIR hyperspectral imaging systems are usually  
59 designed for reflectance measurements, that is, measurements from the top surface of the  
60 sample. To obtain more representative spectral readings from heterogeneous samples,  
61 transmission measurement is an alternative option. The NIR region of the electromagnetic  
62 spectrum is of particular interest in this respect due to the relatively low absorption by  
63 biological soft tissues. Wavelengths shorter than 600nm are strongly absorbed by pigments in  
64 the tissue, wavelengths longer than 1300 nm are strongly absorbed by water,<sup>7</sup> while the 600-  
65 1300 nm spectral region is less absorbed and is often referred to the “tissue optical  
66 window”.<sup>8,9</sup> The favorable spectral properties within this window enable relatively deep  
67 penetration of light in meat and other food products in general. Spectroscopic techniques are  
68 therefore not limited to reflection measurements only, but also transmission becomes possible.

69 The complete thickness of the sample can be probed when NIR radiation is transmitted from  
70 one side to the other. Transmission imaging does, however, pose some substantial challenges.  
71 Although NIR radiation is relatively little absorbed by water, the obtainable transmission  
72 depth in tissues like meat is still limited. Strong light scattering in muscle tissues will also  
73 limit penetration depth. In the case of spectral imaging, scattering can also result in blurred  
74 images with fewer details. Nevertheless, NIR transmission imaging has shown promising  
75 results when applied to mammography, where it is possible to detect internal structures and  
76 also measure oxygenation of the blood in breasts of thicknesses up to 7 cm.<sup>10,11</sup> Consequently,  
77 NIR transmission might be useful for samples that are heterogeneous and limited in thickness.

78 Transmission imaging in the visible and NIR spectral regions has been reported mainly for  
79 detection of internal defects in foods. Ariana and Lu<sup>12</sup> demonstrated this for whole pickles.  
80 Transmission spectral imaging has also been reported to give good results for detection of  
81 nematodes in fish fillets.<sup>2,13</sup> NIR transmission has also been evaluated for quantification of  
82 sugar and acids in individual blueberries, however, the imaging capability in this case was  
83 mainly utilized to detect the berries, not in the spectral analysis.<sup>14</sup>

84 A main criterion for transmission measurements is that the position of detection differs from  
85 that of the illumination. A special case of transmission, called interactance, occurs when both  
86 illumination and detection are carried out on the same side of the sample, but separated by a  
87 short distance so that the detected light has traversed parts of the interior of the product. Such  
88 a setup is used for instance to measure internal properties of fruit by NIR.<sup>15</sup> Interaction  
89 measurements can also be done in imaging mode and is illustrated by Wold et al.,<sup>16</sup> who  
90 showed that it is possible to image the distribution of liver and roe inside live crabs. In that  
91 case, the light probed approximately the upper 10 mm of the sample.

92 It is shown that surface fat distribution in meat can be mapped by NIR hyperspectral imaging  
93 in reflectance mode,<sup>17</sup> and in the upper 15 mm layer in interactance mode.<sup>5</sup> The fat content of  
94 the whole meat sample can then be estimated from the probed region only, and the accuracy  
95 associated with the measurement will thus depend on the homogeneity of the sample. For  
96 heterogeneous meat, it is thus not sufficient to measure surface only, if high accuracy is  
97 required, and X-ray is now being widely used in the meat industry to measure fat content in  
98 boxes of meat as well as in e.g. pork bellies. NIR imaging can also be used on boxes of meat,  
99 and performs well when the surface layer of the meat is representative for the rest of the  
100 box.<sup>18</sup> On the other hand, the fat content in pork bellies is consistently unevenly distributed  
101 with a fatty layer on top of the muscle. Thus, fat classification of pork bellies is difficult using  
102 traditional NIR measurements on only one of the sides, since hardly any of the two sides will  
103 be representative for the whole belly.

104 To our knowledge, chemical imaging of complex foods based on NIR transmission has not  
105 been reported to date. While industrial applications involving on-line interactance  
106 spectroscopy exists,<sup>4,5,16,18</sup> transmission spectroscopy is mostly common in laboratory  
107 equipment, where samples can be properly prepared and presented as part of a measurement  
108 protocol.

109 In this paper we present initial measurements from a setup for NIR transmission imaging  
110 where the samples are completely transilluminated and an NIR imaging scanner is used to  
111 obtain spectral images. The set-up is based on falling samples, meaning rapid movement of  
112 samples and relevant for industrial use. Model samples composed of ground pork meat were  
113 used to illustrate quantitative imaging of fat distribution also when the fat was embedded  
114 inside the samples. It is also shown that promising results can be obtained for whole pork  
115 bellies as well as salmon fillets with skin.

116

## 117 **Materials and Methods**

### 118 **Materials**

119 Three different sets of food samples were prepared for the NIR transmission imaging  
120 experiment.

#### 121 *Ground pork meat*

122 Three model samples were made based on two batches of ground pork meat. One batch was  
123 ground meat with a fat content of 16%, the other batch was ground back fat and held about  
124 80% fat. The three test samples were shaped as rectangular blocks of size approximately 30  
125 cm \* 20 cm \* 3 cm, composed as shown in Figure 1 A-C. In this arrangement, both the  
126 amount and location of the fat were known. Some of the fat was visible at the surface, while  
127 some of the fat was embedded inside the sample. All samples had one side with no visible  
128 high fat areas. Samples were vacuum packed in transparent plastic film to ensure that the  
129 samples were kept stable throughout the experiment.

130 15 calibration samples were made from the two mentioned batches of ground meat. Different  
131 shares of lean and fat were blended in samples of about 500 grams, with a broad variation in  
132 fat. The samples were made as rectangular blocks of thickness 3 cm. Fat content in each  
133 sample was calculated based on the weight ratio of the two materials. The calibration samples  
134 were used to make a simple regression model that could be applied as a reference against the  
135 spectral images from the test samples to illustrate the possibility of quantitative transmission  
136 imaging.

#### 137 *Pork bellies*

138 Two fresh boneless pork bellies were collected from a slaughterhouse. The size of the bellies  
139 was approximately 50 cm \* 35 cm for both, and they weighted about 6 kg. Thickness varied  
140 between about 3 and 5 cm. The outer side of the bellies consisted of the fat rich blubber  
141 covered by the smooth yellowish bacon rind. The inner side was the meat side with an uneven  
142 surface given by the anatomy of the animal (Figure 1 D).

#### 143 *Salmon fillets*

144 Twenty salmon fillets with skin varying in weight from 48-438 g were obtained from 20  
145 farmed salmon slaughtered two days before. The fillets were stored on ice before spectral  
146 measurements. After being measured they were cut in different portions (2, 3 or 4 portions  
147 depending on size), and a total of 69 portions were made with varying size, thickness and  
148 shape. Fat content was determined in each portion by low field NMR. Three example fillets  
149 are shown in figure 1 E.

150

#### 151 **Imaging spectroscopy system**

152 The transmission imaging system was made up of three main components (Figure 2); the light  
153 source, a commercial NIR imaging scanning system (QVision 500, Tomra Sorting Solutions,  
154 Asker, Norway), and a sample holder.

155 QV500 is an NIR imaging system designed for daily industrial on-line spectral imaging of  
156 foods on conveyor belts. The system is designed for non-destructive determination of fat,  
157 protein and water content in ground and chopped meat and is in wide-spread use in meat  
158 processing plants. It collects VIS and NIR spectra in the range 460 – 1040 nm, sampling at  
159 every 20<sup>th</sup> wavelength and thus has a spectral bandwidth of about 20 nm. Under normal  
160 operation, a light beam from an internal light source is scanned rapidly across the conveyor

161 belt. The field of detection is about 1 cm away from the light beam spot, so interactance  
162 measurements with typical probing depth of 15 mm are obtained, depending on the type of  
163 sample being measured. Based on the scanning and the movement of the belt, a hyperspectral  
164 image is constructed. Typical pixel size is about 5 mm\*5mm. An early version of the system  
165 is described by Wold et al.<sup>16</sup>

166 In the present work, a modified version of the QV500 scanning system was used. The internal  
167 light source was turned off, and replaced with an external light source positioned on the other  
168 side of the sample, thus providing a light transmission setup.

169 The external light source consisted of two tube halogen lamps (OSRAM 64784 Haloline 2000  
170 W), mounted in an aluminum frame, inside two parabolic mirrors to focus the light along one  
171 line on the sample. A potentiometer was used to adjust the power of the lamp. Higher light  
172 intensity was needed to obtain sufficient signals from the meat model samples, than from the  
173 salmon fillets. The high power of the lamp required rapid movement of the samples to avoid  
174 heating.

175 Sample movement was vertical. A tall frame (2 m high) was made with a pulley at the top. A  
176 rope went through the pulley and was connected to a horizontal rack that could be adjusted to  
177 hoist up and down. The sample was attached to the rack with metal clips so that it could be  
178 moved vertically. During scanning, the speed of the samples was close to free fall. Scanning  
179 time per sample was typically 1 sec.

180 The salmon fillets were measured also in interactance mode. The external lamp was switched  
181 off, and the internal lamp was used as normal for the scanner. The interactance measurements  
182 were also done on vertically moving fillets.

183



## 184 **Image processing and data analysis**

185 There are several ways to calibrate an NIR imaging system. In this case, we used the mean  
186 NIR spectra from each of the calibration samples (the 15 meat samples and the 69 salmon  
187 samples), and these were used to make a calibration against fat content for each of the two  
188 products. A segmentation criterion for meat/fish based on spectral characteristics was  
189 developed in order to automatically detect the sample and to extract the spectral data.  
190 From each calibration sample we obtained an average intensity NIR spectrum (T). This  
191 spectrum was converted to an absorption spectrum ( $\log_{10}(1/T)$ ) to make the data more linear.  
192 The spectral shape was affected by optical properties such as color, sample physical  
193 properties, sample distance from the scanner, as well as thickness of sample. To remove some  
194 of the spectral variation connected to these properties, standard normal variate (SNV) was  
195 applied to normalize the data; subtract the mean of the spectrum from each wavelength in the  
196 spectrum and divide by the standard deviation of the spectrum.<sup>19</sup>  
197 Spectral data from the salmon portions was obtained in the following way: The spectral  
198 images were compared and aligned with the portion images (Figure 1E). The portions were  
199 then manually outlined in the spectral images by an image processing tool. The average  
200 spectrum was calculated for each portion.

201

202 Partial least squares regression (PLSR)<sup>20</sup> was used to make the calibration between NIR  
203 spectra and fat concentration for the two calibration sets. Full cross validation was applied to  
204 determine the optimal number of PLS factors and to evaluate the predictive ability of the  
205 models. The prediction error was estimated by the root mean square error of cross validation  
206 (RMSECV) where  $\hat{y}_i$  is the predicted value from the cross validation,  $y_i$  is the reference value  
207 and  $i$  denotes the samples from 1 to  $N$ .

208

209

210

$$RMSECV = \sqrt{\frac{1}{N} \sum_{i=1}^N (y_i - \hat{y}_i)^2}$$

211

212 The resulting regression vectors were applied at pixel level in the hyperspectral images to  
213 obtain fat distribution maps in the model samples and in the salmon fillets. To avoid  
214 overoptimistic results, portions from the fillets to be estimated were not used in the regression  
215 model. The regression vector for fat in ground pork was also applied on the pork bellies.

216 Principal component analysis (PCA)<sup>20</sup> was also used on the spectral dimension of the spectral  
217 images to investigate the main spectral components and how these were distributed in the  
218 samples.

219 The software The Unscrambler ver. 9.8 (CAMO Software AS, Oslo, Norway) was used for  
220 regression analysis. All image processing of multispectral images; sample segmentation,  
221 spectral extraction, spectral pre-processing, and generation of chemical images were carried  
222 out by the use of MATLAB version 7.10 (The MathWorks Inc., Natic, MA).

223

## 224 **Reference measurements**

225 Reference measurements for fat were conducted for all the 69 salmon fillet portions and for  
226 the lean and the fat fractions of pork meat. Five parallels from each sample were subjected to  
227 fat measurements. The average values of the parallels were used in the calibration work. The  
228 fat content was determined by low field proton nuclear magnetic resonance (NMR), using the  
229 Maran Ultra Resonance 0.5 T (Oxford Instruments, UK) equipped with a gradient probe. The

230 method used was “The oneshot method” developed by Anvendt Teknologi AS (Harstad,  
231 Norway).<sup>21</sup> Operating temperature of the magnet was 40°C and the samples were heated up to  
232 this temperature before measurement to ensure that the fat was in liquid form. The weight of  
233 the meat samples was measured and calibration was done against a reference meat sample of  
234 known weight containing 14.3% fat (SMRD 2000 Matrix Meat Reference Material, National  
235 food Administration, Uppsala, Sweden). Salmon oil was used to calibrate the instrument prior  
236 to analysis of the salmon samples.

237

## 238 **Results and discussion**

### 239 *Spectral features*

240 Figure 3a shows an intensity image for one channel (940 nm) of a salmon fillet. The main  
241 intensity variation in the image was caused by thickness differences. The lowest values can be  
242 seen to the upper left where the fillet was at its thickest, intensity increased towards the tail  
243 where the fillet was thinner. The thinner belly was also higher in intensity. At the tail it can be  
244 seen that the right part had higher intensity than the left part. This is due to color variation in  
245 the skin. The skin is dark on the upper part of fish and light/silver on the belly side. The dark  
246 skin will absorb more NIR light than the light skin, in particular at wavelengths close to the  
247 visible region. The high intensity at the upper part of the fillet (at the neck) was mainly due to  
248 a kind of optical reflections that appeared at the upper edge of some samples.

249 The intensity variations in the image result in correspondingly large offset variations in the  
250 NIR spectra (Figure 3b). Spectra from the thick part of the fillet had overall higher absorbance  
251 values than those from thinner parts. A spectrum from left tail had higher absorption than the  
252 one from right tail due to the darker skin. Spectra from thicker parts also have higher

253 difference in absorption between different wavelengths (higher contrast); longer pathlength  
254 gives more distinct spectral features.

255 The peak/shoulder at about 930 nm stems from fat (third overtone of CH stretch), the broad  
256 peak at 980 nm is absorption by water (second overtone of OH stretch), while the variation  
257 towards the visible region is much due to color variations related to skin, color and darkness  
258 of meat.<sup>22</sup> In the spectrum from the front part of the belly the fat absorption at 930 nm can be  
259 distinguished as a clear shoulder, while from the leaner loin the spectrum is dominated by the  
260 large water peak.

261

262 After spectral normalization, the offset variation was removed and the spectra had the same  
263 internal contrast (Figure 3c). The fat variation around 930 nm was then clearer. The spectra  
264 from the thin tail differ from the others by relatively strong absorption towards the visible,  
265 and this is probably because the skin contributes to a relatively larger part of the optical  
266 pathway.

267 PCA is an efficient way to visualize how the main spectral properties are distributed in  
268 spectral images. Figure 4 shows the spectral loadings for the first four principal components  
269 (4e) and how the corresponding scores from these components are distributed in a salmon  
270 fillet. The PCA was performed on non-normalized absorption spectra. The first component is  
271 a pure offset component and reflects the thickness of the sample. The scores from the second  
272 component is quite similar to the first and are probably related to spectral contrast; the thicker  
273 the sample is, the higher contrast in the spectra. The third component seems to some extent to  
274 separate between dark and silver part of skin. This matches with the loading spectrum, which  
275 expresses the large variation towards the visible part of the spectrum. The fourth component is  
276 related to fat content with its notable fat peak in the loadings, and the score image highlights  
277 the fat belly as well as the fat rich dark muscle along the lateral line just under the skin.

278

279 The transmission images apparently contain much information, and the spectral properties are  
280 typical for NIR spectra from muscle foods. The spectra from the pork meat samples had  
281 mainly the same properties as those from salmon and were similar to spectra obtained in  
282 interactance mode.<sup>5,18</sup>

283

#### 284 *Calibration*

285 Fat content in the lean and fat pork batches were 16% and 80% of the wet weight,  
286 respectively. When these were combined in 15 different calibration samples, the fat content  
287 varied gradually from 16% to 80 %. Fat content in the 69 salmon portions varied from 6.5%  
288 to 31.5%, the mean value was 16.7% and standard deviation was 5.4.

289

290 Both data sets had a spread in fat content that was suitable for regression modelling. Table 1  
291 summarizes the model results. The model for ground pork meat obtained high correlation  
292 between actual and estimated fat content and a prediction error of about 3.6%. The result is  
293 comparable with a model obtained with the same system in interactance mode on intact pork  
294 meat,<sup>5</sup> where a RMSECV of 3.0% was obtained. In that case a larger sample volume was  
295 scanned per calibration sample.

296 The model for fat in salmon fillet portions did also obtain a high correlation and rather low  
297 prediction error. The results demonstrate that it is possible to make quantitative models based  
298 on NIR transmission data. Variation in thickness is probably introducing some unwanted  
299 spectral variation, however, in the salmon system where thickness varied from 0.6 cm to 4 cm  
300 it was still possible to obtain a good model.

301 It is interesting to compare with the model obtained on interactance measurements on the  
302 same fillets. This model had lower correlation and correspondingly a higher prediction error.

303 The main difference between the data is that in interactance mode, only about the upper 15  
304 mm layer was probed. It is well known that most of the fat is located beneath the skin,<sup>23</sup> and  
305 interactance measurements will not reach these regions where the fillets are thicker than 15  
306 mm, while transmission measurements will capture spectral information that is representative  
307 for the full sample thickness. The interactance system is optimized to operate above a  
308 conveyor belt where fillets have a fixed distance to the scanner. In the present free-falling  
309 system there was also some horizontal movement, which resulted in variation in distance  
310 between scanner and sample. Interaction measurements might be more sensitive to such  
311 movements than transmission measurements are.

312

### 313 *Chemical images*

314 The regression vectors obtained by calibration were applied pixel by pixel in the hyperspectral  
315 images to estimate fat values based on the pixel spectra, as well as average fat contents for  
316 each sample. In that way images of fat distribution were constructed. The regression vectors  
317 are shown in Figure 5. Both vectors emphasizes the fat peak at around 930 nm.

318 Estimated fat images of the pork model samples shown in Figure 1 A-C are shown in Figure  
319 6. Two images for each sample are shown; one based on scan with front of sample facing  
320 scanner, the other with back side of sample facing scanner. From Figure 1 it can be seen that  
321 no high fat regions were visible on any of the back sides, while the front sides exposed high  
322 fat parts. The most important result here is that the fat images looked mostly the same,  
323 independent of sample side facing the scanner. The predicted fat values at pixel level were  
324 close to the actual fat contents in the model samples. It can also be seen that the average fat  
325 contents obtained per sample were very similar irrespective of orientation. This is what we  
326 would expect from a well working transmission imaging system. The images confirm that it is

327 possible to make quantitative chemical images based on NIR that maps internal properties of  
328 rather thick samples.

329 For sample A it can be noted that that the visible fat region in the lower right on the front part  
330 was easily seen in the fat image when the front side of the sample faced the scanner. When the  
331 back side faced the scanner, this part was not possible to discern. The large rectangular fatty  
332 area in the upper left corner of sample A was visible from back side but less intense compared  
333 to front side. This effect is most likely due to light scattering. Details on the surface facing the  
334 light source get blurred as the light propagates through the sample. Details on the sample  
335 surface facing the scanner on the other side, is less obscured by light scattering. Although  
336 some of the spatial information is obscured during transmission, the chemical signals from the  
337 fat are preserved as the total estimated fat content remains the same.

338

339 Figure 7 shows a similar example with the whole pork bellies. We did not have a regression  
340 model optimized for intact pork meat. However, by using the model for ground pork it could  
341 be illustrated again that estimated average fat content was almost the same, independent of  
342 which way the belly was scanned. When the relatively flat rind side of the belly faced the  
343 scanner, the resulting fat image showed the overall variation in fat across the belly. With the  
344 meat side (as shown in Figure 1D) against the scanner, the same overall fat variation could be  
345 seen, but also details of the fat distribution on the meat side. The differences in the fat images  
346 are again due to the effect of light scattering.

347 Figure 8 shows estimated fat images of three salmon fillets with skin. The score images of one  
348 fillet shown in Figure 4 illustrated the huge and systematic spectral variation that is present in  
349 these samples. In spite of these variations across the fillets, the regression vector seemed to  
350 produce fat images that reflect the typical fat concentrations and distribution in salmon. The  
351 average fat values obtained for each fillet corresponded well with the reference values.

352 **General discussion**

353 The results confirm that it is possible, and also valuable, to perform hyperspectral  
354 transmission imaging on meat samples of thickness up to at least 5 cm. Quantitative imaging  
355 of internal chemical composition is feasible, even when samples varies in thickness or are  
356 covered with skin or rind, as with the salmon fillets and pork bellies, respectively.

357 Sample thickness is a main limiting factor, and at some point an increased thickness will  
358 result in signals, which are too weak or noisy to be useful. Before we made the ground pork  
359 samples of 3 cm thickness, we made an effort with similar samples of 5 cm thickness. In that  
360 case, the signals were too low and spectral shape distorted. Better signals were obtained on  
361 the 5 cm thick pork bellies, probably due to less light absorption and light scattering. It  
362 illustrates that critical thickness will vary from product to product.

363 Another issue is variation in thickness within the samples. It is important to adjust the lamp  
364 intensity so that signals from both thin and thick parts of the sample are applicable and not  
365 distorted by either noise or detector saturation. For the salmon fillets, for instance, the lamp  
366 intensity was adjusted to give useful spectral readings for thin bellies (0.5 cm thick) and the  
367 thicker loin part (up to 4 cm thick). Fillets measured without skin (not presented here)  
368 required less light intensity than fillets with skin.

369 In this work we used SNV prior to calibration to remove the largest spectral variation  
370 connected to variation in thickness. Since the signals at every pixel is heavily dependent on  
371 thickness, it would probably be possible to use this information to optimize spectral pre-  
372 processing, and also improve pixel predictions as well as the predicted average values. A  
373 thick part of a sample will have more weight than a thin part in a weighted average.

374 Pork bellies and salmon fillets are not ideal for a free falling sample system. The lab system  
375 was constructed for vertical sample movement for convenience. Free falling samples are used



376 in many optical sensor systems for food, however, transmission measurements for larger  
377 samples can also be implemented on e.g. conveyor belts separated with narrow slits.

378

### 379 **Acknowledgements**

380 The research presented here was funded by the Norwegian Research Council through the  
381 project CYCLE (225349/E40) and the Norwegian Agricultural Food Research Foundation.  
382 The financial support is greatly acknowledged by the authors. Bjørg Narum and Karen  
383 Wahlstrøm Sanden are thanked for skilled technical assistance.

384

385

### 386 **References**

- 387 1. A.H. Sivertsen, C.K. Chub, L.C. Wang, F. Godtliebsen, K. Heia, H. Nilsen. “Ridge  
388 detection with application to automatic fish fillet inspection”. *J. Food Eng.* 2009. 90(3):  
389 317–324.
- 390 2. K. Heia, A.H. Sivertsen, S.K. Stormo, E. Elvevoll, J.P. Wold, H. Nilsen. “Detection of  
391 Nematodes in Cod (*Gadus morhua*) Fillets by Imaging Spectroscopy“. 2007. *J. Food Sci.*  
392 72(1): E11-E15.
- 393 3. D. Airado-Rodríguez, M. Høy, J. Skaret, J.P. Wold. “From multispectral imaging of  
394 autofluorescence to chemical and sensory images of lipid oxidation in cod caviar paste”.  
395 *Talanta.* 2014. 122: 70–79.
- 396 4. V.H. Segtnan, M. Høy, F. Lundby, N. Narum, J.P. Wold.. “Fat distributional analysis in  
397 salmon fillets using non-contact near infrared interactance imaging: A sampling and  
398 calibration strategy“. 2009. *J. Near Infrared Spectrosc.* 17(5): 247-253.

- 399 5. J.P. Wold, M. O'Farrel, M. Høy, J. Tschudi. "On-line determination and control of fat  
400 content in batches of beef trimmings by NIR imaging spectroscopy". 2011. *Meat Sci.*  
401 89(3): 317-324.
- 402 6. I. Måge, J.P. Wold, F. Bjerke, V.H. Segtnan. "On-line sorting of meat trimmings into  
403 targeted fat categories". 2013. *J. Food Eng.* 115 (3): 306-313.
- 404 7. C.L. Tsai, J.C. Chen, W.J. Wang. "Near-infrared Absorption Property of Biological Soft  
405 Tissue Constituents". 2001. *J. Med. Biol. Eng.* 21(1): 7-14.
- 406 8. O.W. Van Assendelft. *Spectrophotometry of hemoglobin derivatives*, Royal Vangorcum  
407 Ltd., Assen, The Netherlands, 1970.
- 408 9. J.A. Curcio, C.C. Petty. "The near infrared spectrum of liquid water". 1951. *J. Opt. Soc.*  
409 *Am.* 41(5): 302-304.
- 410 10. Y. Yu, N. Liu, A. Sassaroli, S. Fantini. "Near-infrared spectral imaging of the female  
411 breast for quantitative oximetry in optical mammography". 2009. *Appl. Opt.* 48(10):  
412 D225-D235.
- 413 11. Y. Yu, A. Sassaroli, D.K. Chen, M.J. Homer, R.A. Graham, S. Fantini. "Near-infrared,  
414 broad-band spectral imaging of the human breast for quantitative oximetry: Applications to  
415 health and cancerous breasts". *J. Innovative Opt. Health Sci.* 2010. 3(4): 267–277.
- 416 12. D.P. Ariana, R. Lu. "Evaluation of internal defect and surface color of whole pickles using  
417 hyperspectral imaging". *J. Food Eng.* 2010. 96(4): 583–590.
- 418 13. J.P. Wold, F. Westad, K. Heia. "Detection of parasites in cod fillets by using SIMCA  
419 classification in multispectral images in the visible and NIR region". *Appl. Spectrosc.*  
420 2010. 55(8): 1025-1034.

- 421 14. G.A. Leiva-Valenzuela, R. Lu, J.M. Aguilera. "Assessment of internal quality of  
422 blueberries using hyperspectral transmittance and reflectance images with whole spectra or  
423 selected wavelengths". *Innovative Food Sci. Emerging Technol.* 2014. 24: 2-13.
- 424 15. C.V. Greensill, K.B. Walsh. "A remote acceptance probe and illumination configuration  
425 for spectral assessment of internal attributes of intact fruit". *Meas. Sci. Technol.* 2000.  
426 11(12): 1674.
- 427 16. J.P. Wold, M. Kermit, A Woll. "Rapid nondestructive determination of edible meat  
428 content in crabs (*Cancer Pagurus*) ny Near-Infrared Imaging spectroscopy". *Appl.*  
429 *Spectrosc.* 2010. 64 (7): 691-699.
- 430 17.M. Kamruzzamana, G. ElMasry, D.W. Sun, P. Allen. "Non-destructive prediction and  
431 visualization of chemical composition in lamb meat using NIR hyperspectral imaging and  
432 multivariate regression". *Innovative Food Sci. Emerging Technol.* 2012. 16: 218–226.
- 433 18. M. O'Farrell, J.P. Wold, M. Høy, J. Tschudi, H. Schulerud. "On-line fat content  
434 classification of inhomogeneous pork trimmings using multispectral near infrared  
435 interactance imaging". *J. Near Infrared Spectrosc.* 2010. 18(2): 135-146.
- 436 19.R.J. Barnes, M.S. Dhanoa, S.J. Lister. "Standard Normal Variate Transformation and De-  
437 trending of Near-Infrared Diffuse Reflectance Spectra". *Appl. Spectrosc.* 1989. 43(5): 772-  
438 777.
- 439 20. H. Martens, T. Næs. *Multivariate calibration.* John Wiley and Sons, Chichester, UK. 1989
- 440 21. G.H. Sørland, P.M. Larsen, F. Lundby, A.P. Rudi, T. Guiheneuf. "Determination of Total  
441 Fat and Moisture Content in Meat Using Low Field NMR", *Meat Sci.* 2004. 66 (3): 543–  
442 550.

443 22. L. Weyer, S.C. Lo. "Spectral structure correlations in the near infrared". In J. M.  
444 Chalmers and P. R. Griffiths, editors. Handbook of Vibrational Spectroscopy. Chichester,  
445 UK: John Wiley & Sons Ltd, 2002, p.1817-1837.

446 23. M. Rye, G. Baeverfjord, M. Jopson. "Computerized tomography can be used for  
447 evaluation of lipid distribution in market-sized Atlantic salmon". Europ. Aquacult. Soc.  
448 Special Publ. 1995. 23: 387-388.

449

450

451 **Figure captions**

452 **Figure 1** A-C shows front, back and cross section of model samples composed of ground  
453 pork meat. D) Meat side of one of the pork bellies. E) Example of salmon fillets cut in  
454 portions of different shapes, sizes and thicknesses.

455 **Figure 2** Setup for transmission imaging system. It was based on vertical movement (free  
456 fall) of the samples between light source and NIR imaging scanner.

457 **Figure 3** a) Intensity image of salmon fillet at 940 nm. Numbers in image corresponds to  
458 spectra in b) and c). b) Absorption spectra from numbered (1-6) pixels in intensity image. c)  
459 Same spectra, SNV corrected.

460 **Figure 4** a-d) Score images for principal components 1-4 based on one single salmon fillet. e)  
461 Corresponding loadings 1 (blue), 2 (green), 3 (red) and 4 (cyan).

462 **Figure 5** Regression coefficients for fat in salmon fillets (dashed) and ground pork  
463 (solid)

464 **Figure 6** Images of predicted fat distribution in model samples A-C (shown in Figure 1)  
465 measured with front and back side facing NIR scanner. Estimated average fat content  
466 indicated above each image.

467 **Figure 7** Images of predicted fat distribution in two pork bellies (A and B) measured with  
468 front and back side facing NIR scanner. Estimated average fat content indicated above each  
469 image.

470 **Figure 8** Images of predicted fat distribution in salmon fillets with skin. M: Measured average  
471 fat content by reference method, P: Estimated average fat content by NIR imaging.

472

473

474

475

476

477 **Table I** Regression results for PLSR calibrations for fat. # PLS factors: Number of litem  
478 variables used in the model, R: correlation between estimated and measured fat content,  
479 RMSECV: Root mean square error of cross validation.

Data	# PLS factors	R	RMSECV (%)
Pork meat	5	0.98	3.67
Salmon transmission	4	0.95	1.68
Salmon interactance	3	0.89	2.41

480

481

482 **Figures**

483

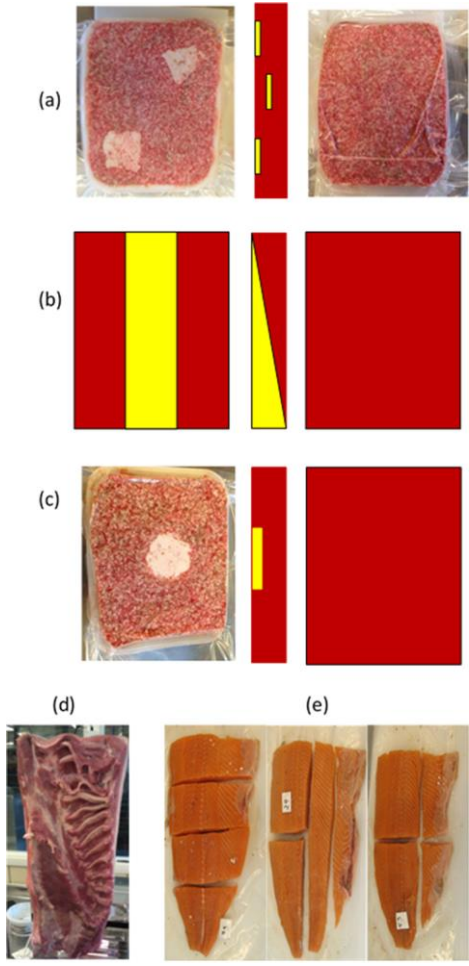
484

485

486 **Figure 1**

487

488



489

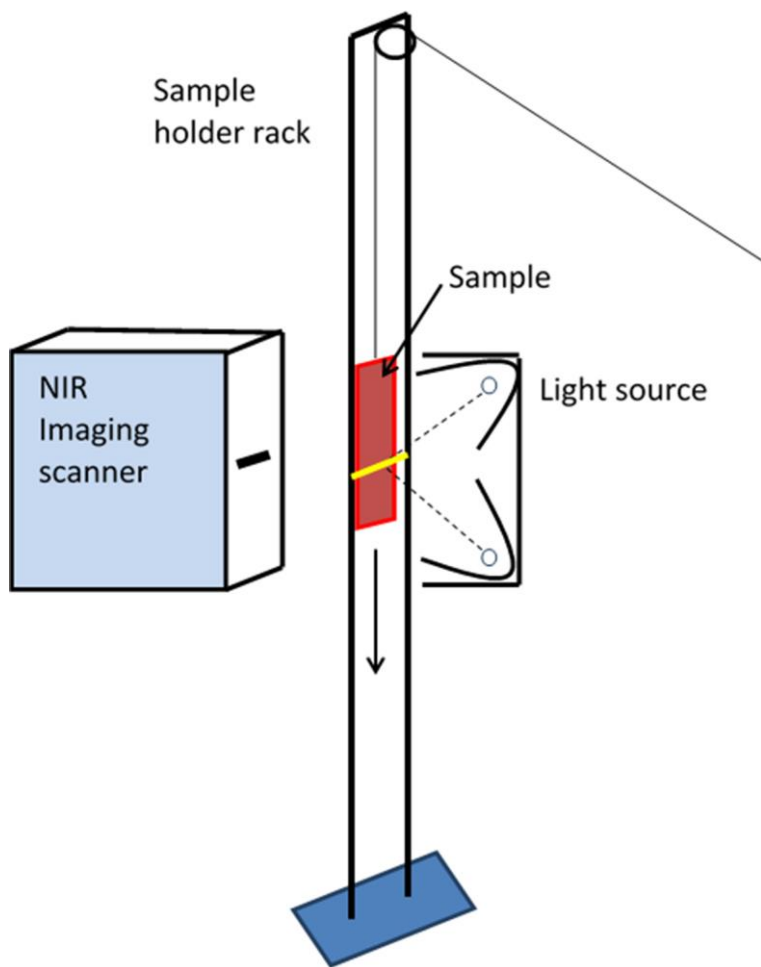
490

491



492 **Figure 2**

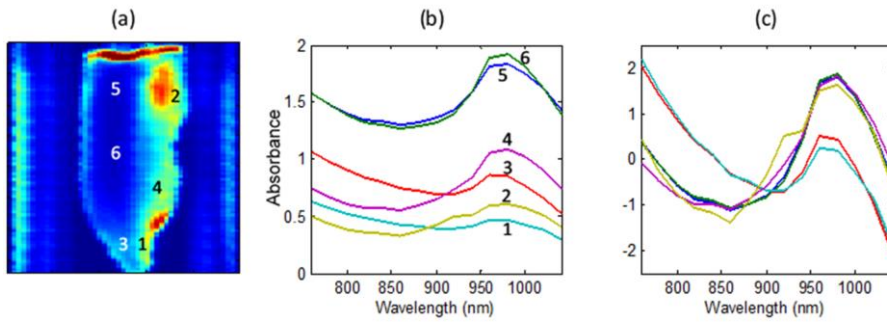
493



494  
495  
496  
497  
498  
499  
500  
501  
502  
503  
504  
505  
506  
507  
508  
509  
510  
511  
512  
513  
514  
515

516  
517  
518  
519  
520  
521

**Figure 3**

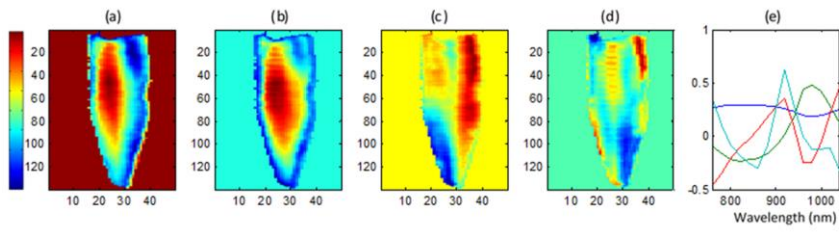


522  
523  
524  
525  
526  
527  
528  
529  
530  
531

532 **Figure 4**

533

534



535

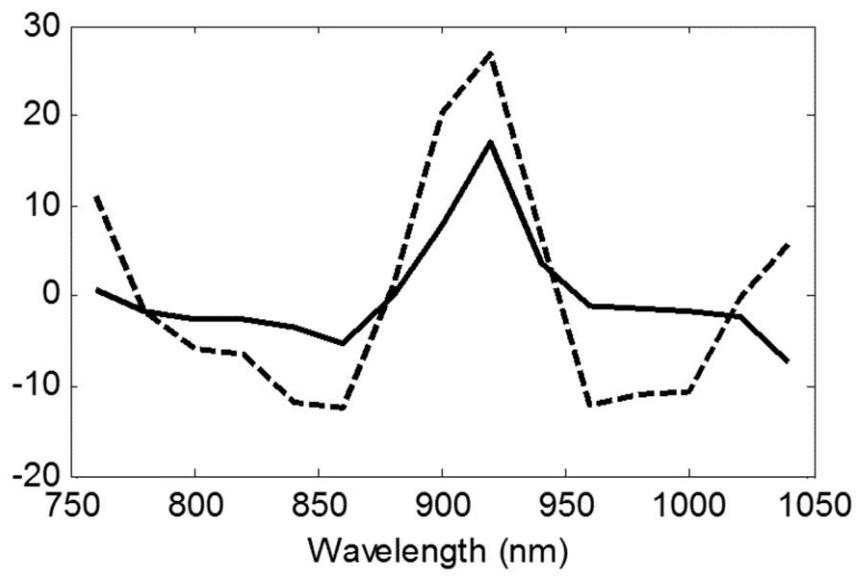
536

537

538

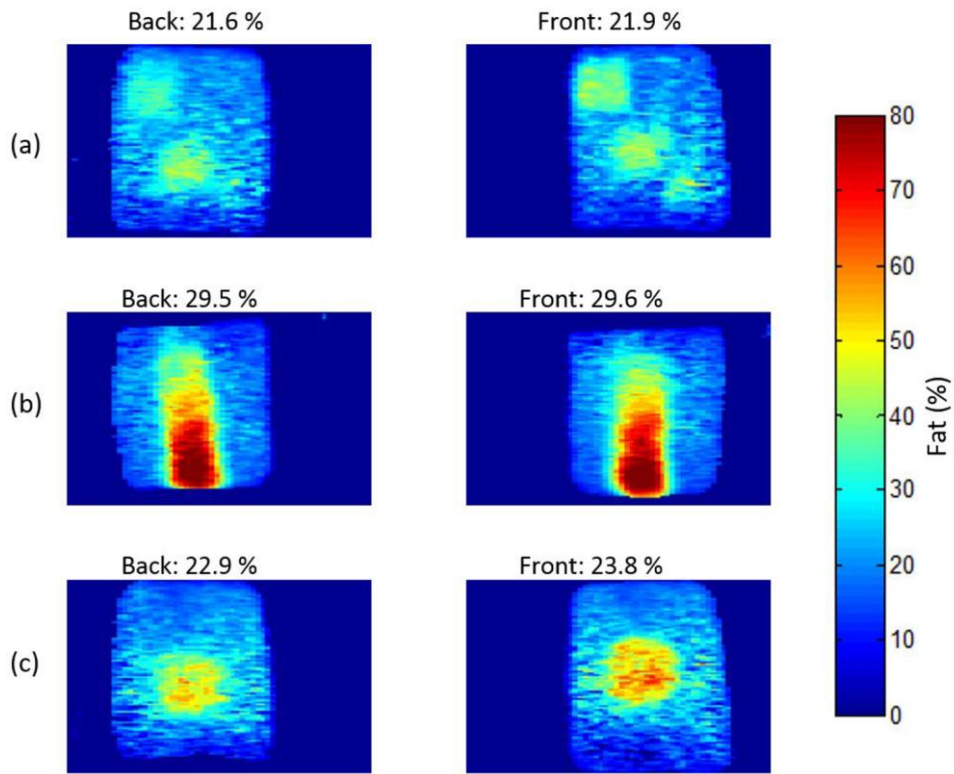
539

540  
541



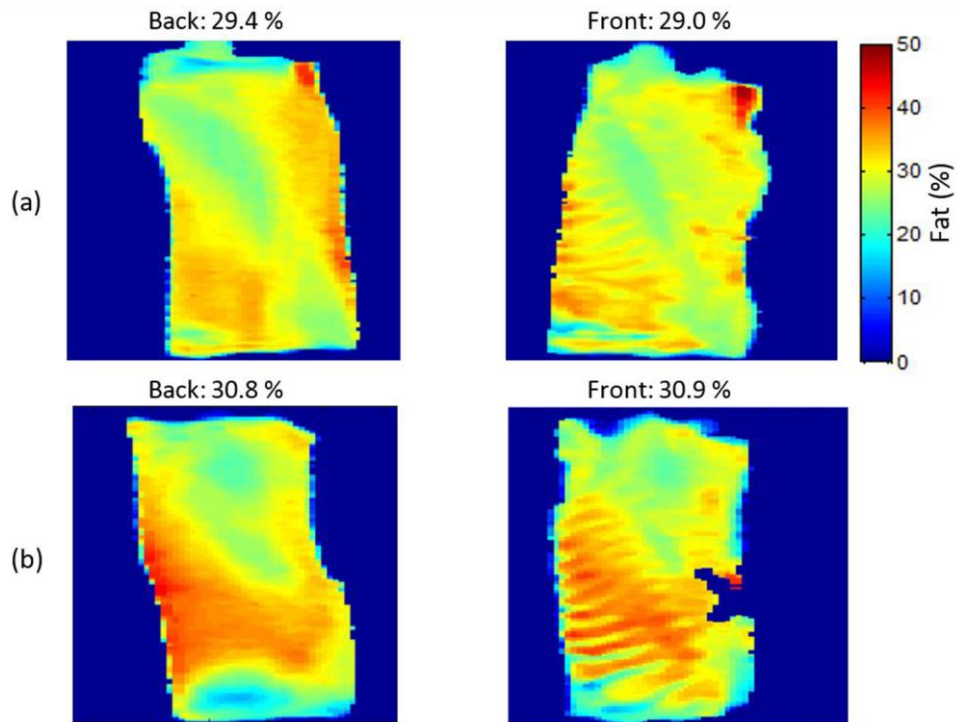
542 **Figure 5**  
543  
544  
545

546 **Figure 6**  
547



548  
549  
550  
551  
552  
553

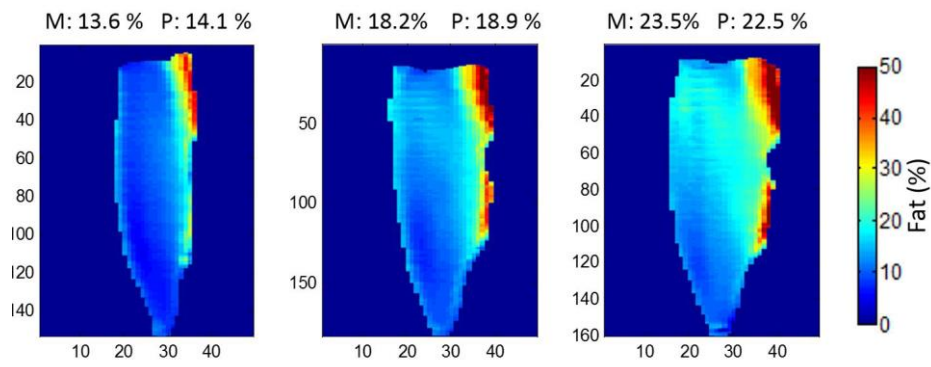
554 **Figure 7**  
555



556  
557  
558

559 **Figure 8**

560



561

562

563

564

565

566

567

568

569

570

571

572

573

574

575

576

577

578

579

580

581